




Article

# Electrochemistry of Inorganic OCT-PbS/HDA and OCT-PbS Photosensitizers Thermalized from Bis(*N*-diisopropyl-*N*-octyldithiocarbamate) Pb(II) Molecular Precursors

Mojeed A. Agoro <sup>1,2,\*</sup> , Johannes Z. Mbese <sup>1,\*</sup>  and Edson L. Meyer <sup>2</sup> <sup>1</sup> Department of Chemistry, University of Fort Hare, Private Bag X1314, Alice 5700, South Africa<sup>2</sup> Fort Hare Institute of Technology, University of Fort Hare, Private Bag X1314, Alice 5700, South Africa; emeyer@ufh.ac.za

\* Correspondence: magoro@ufh.ac.za (M.A.A.); jmbese@ufh.ac.za (J.Z.M.)

Received: 16 March 2020; Accepted: 13 April 2020; Published: 21 April 2020



**Abstract:** Inorganic nanocrystal solar cells have been tagged as the next generation of synthesizers that have the potential to break new ground in photovoltaic cells. This synthetic route offers a safe, easy and cost-effective method of achieving the desired material. The present work investigates the synthesis of inorganic PbS sensitizers through a molecular precursor route and their impact on improving the conversion efficiency in photovoltaic cells. PbS photosensitizers were deposited on TiO<sub>2</sub> by direct deposition, and their structure, morphologies and electrocatalytic properties were examined. The X-ray diffraction (XRD) confirms PbS nanocrystal structure and the atomic force microscopy (AFM) displays the crystalline phase of uniform size and distribution of PbS, indicating compact surface nanoparticles. The electrocatalytic activity by lead sulfide, using *N*-di-isopropyl-*N*-octyldithiocarbamate (OCT) without hexadecylamine (HDA) capping (OCT-PbS) was very low in HI-30 electrolyte, due to its overpotential, while lead sulfide with OCT and HDA-capped (OCT-PbS/HDA) sensitizer exhibited significant electrocatalytic activity with moderate current peaks due to a considerable amount of reversibility. The OCT-PbS sensitizer exhibited a strong resistance interaction with the electrolyte, indicating very poor catalytic activity compared to the OCT-PbS/HDA sensitizer. The values of the open-circuit voltage ( $V_{OC}$ ) were ~0.52 V, with a fill factor of 0.33 for OCT-PbS/HDA. The better conversion efficiency displayed by OCT-PbS/HDA is due to its nanoporous nature which improves the device performance and stability.

**Keywords:** semiconductor; molecular precursor; thermal-decomposition; electrochemistry; photovoltaic cells

## 1. Introduction

Research into clean energy has been one of the main concerns of material scientists. The release of environmental pollutants, such as CO<sub>2</sub>, through the use of fossil fuels, has heightened the need for renewable solar energy. The amount of sunlight energy released on a daily basis is more than sufficient if the absorbed photons are completely utilized [1]. Apart from the need for new materials for clean energy, more effort is placed on the synthetic pathways that will deal with the shortfall in the solar cells' poor conversion efficiency. Limitations, like defects on the nanomaterial surface through impurities emanating from capping agents and lack of control over the particle size, impede composite transport of the charge carriers [1,2]. This has placed a great deal of emphasis on the fabrication process of photovoltaic cells that will result in better conversion efficiency than the ideal dye sensitizer solar cells (DSSC) (see Figure 1), which have been used over the past two decades. The emergence of quantum

dots (QDs) sensitizer has found great relevance in the formation of many cells, such as inorganic cells, organic cells, solution-process colloidal solar cells and dye-sensitized solar cells [1,3–7]. Their unique size distribution and spectra properties enable them to absorb the entire visible spectrum, resulting in an improved power conversion efficiency. The use of metals or semiconductors that will produce a smaller bandgap and good optical properties is a major prerequisite.

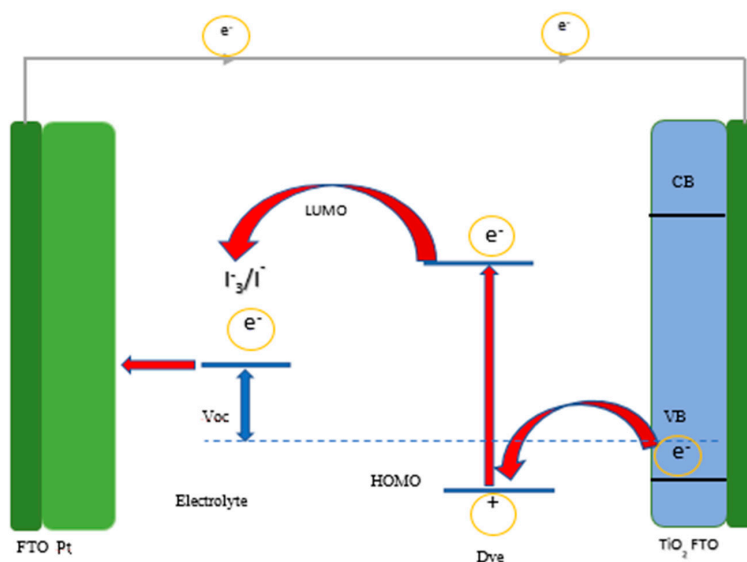


**Figure 1.** Schematic illustration of ideal dye sensitizer solar cells (DSSC).

Inorganic nanocrystal solar cells have been tagged as the next generation of sensitizers that have the potential to break new ground, using semiconductors such as PbS [8]. The adoption of PbS QDs is linked to their near-infrared region properties and excellent photosensitivity, which have made them a better nanomaterial for photovoltaic cells [8,9]. Their direct bandgap of 0.41 eV, high dielectric constant and large exciton Bohr radius (18 nm), have also contributed to their wide application in the production of various items such as photonics, photographic equipment, thermoelectric devices, solar cells and optical fields [10–14]. As diverse applications of PbS QDs in various fields continue to rise, their formation pathways have become a major concern for the material scientist. Various synthetic routes for the fabrication of PbS QDs have been well-documented, such as chemical bath deposition, UV rays, thermal decomposition, microbes and the sonochemical approach [10,15–18]. These have given rise to various shapes, sizes and morphologies of PbS QDs. Therefore, inorganic nanocrystals are seen as having a major advantage because, with the aid of a few compounds, they offer a safe, easy and cost-effective route to form the desired PbS QD. The interesting chemical properties obtained from the use of dithiocarbamate complexes account for their applications in various fields. In addition to their wide application in the realm of materials science, they offer different arrays of anisotropic and isotropic nanomaterials [19–21]. In addition to their wide application, dithiocarbamate complexes offer a clean, nanometric dimension with no impurities when they undergo thermal decomposition [22]. The thermolysis of these metal complexes is one of the easiest and most cost-friendly techniques available for the fabrication of nanoparticles with tunable shapes, minimal defects in structure and narrow size distribution through the aid of capping agents [23,24]. Thermolysis offers various benefits such as controlled conditions, good morphology, purity, environmental friendliness and size distribution [25]. Capping agents, such as hexadecylamine (HDA), trioctylphosphine (TOP) and trioctylphosphine oxide (TOPO), offer excellent surface passivation, stability and better morphology with organic solvents for nanoparticles [26]. The injection of HDA capping agent provides better particle size and morphology that will enhance the efficiency of the fabricated cells [27]. This work employed molecular precursor techniques to fabricate the photosensitizer with the aid of HDA capping agents, in order to control the structural properties, size distribution and morphologies. Direct

deposition was used to coat electrodes with the photosensitizer by immersing them in a solution for a period of time.

## 2. Results and Discussion

### 2.1. X-Ray Diffraction

The XRD patterns of OCT-PbS/HDA and OCT-PbS photosensitizers are illustrated in Figure 2. Furthermore, the phase structure and purity of OCT-PbS/HDA and OCT-PbS were examined by the XRD analysis. The  $2\theta$  values at 19.05, 26.03, 27.03, 34.05, 38.05, 48.07, 52.03, 55.06, 62.04, 66.04, 79.02 and 81.06° are for OCT-PbS. The peak values at 27.03, 31.01, 34.06, 38.05, 52.02, 55.05, 62.05, 66.05, 79.01 and 81.09° are for OCT-PbS/HDA. They both correspond to their crystalline planes of card file No. JCPDC-5-0592 with the diffraction peaks corresponding to (200), (111), (220), (311), (222), (400), (331), (420) and (422) Miller indices. These peaks affirm the PbS QD structure and further confirm the AFM analysis as evidence of successful fabrication of crystalline PbS QDs. The structural disorder emanating from the lattice strain is due to shifts in the diffraction lines. These shifts are typical reflections associated with incorporation into the crystal lattice [28–32].

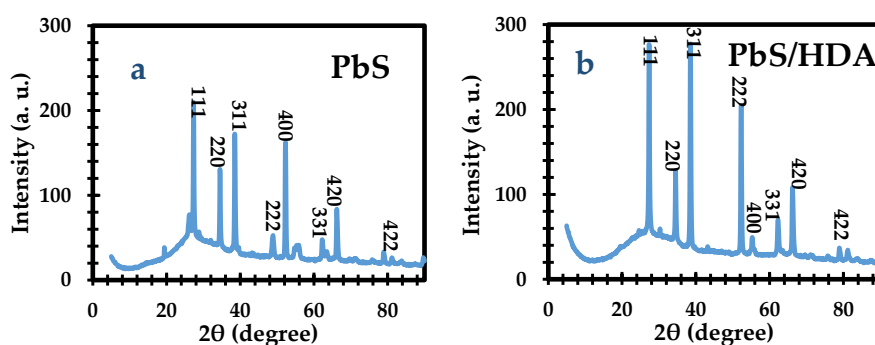


Figure 2. The X-ray diffraction (XRD) spectra of (a) OCT-PbS and (b) OCT-PbS/HDA nanoparticles.

### 2.2. HRTEM

The HRTEM images of OCT-PbS and OCT-PbS/HDA as seen in Figure 3 display crystalline sizes for OCT-PbS between 3.16–5.95 nm and OCT-PbS/HDA within 1.82–2.44 nm, with d-spacing of 2.438 and 3.623 nm, respectively. This is consistent with the previous report on d-spacing for PbS [33,34]. The lattice fringe pattern of both materials can be attributed to their polycrystalline nature. The SAED of OCT-PbS and OCT-PbS/HDA indicated a pattern with grain running in various planes, affirming polycrystalline nature typical of the phenomenon of PbS nanoparticles.

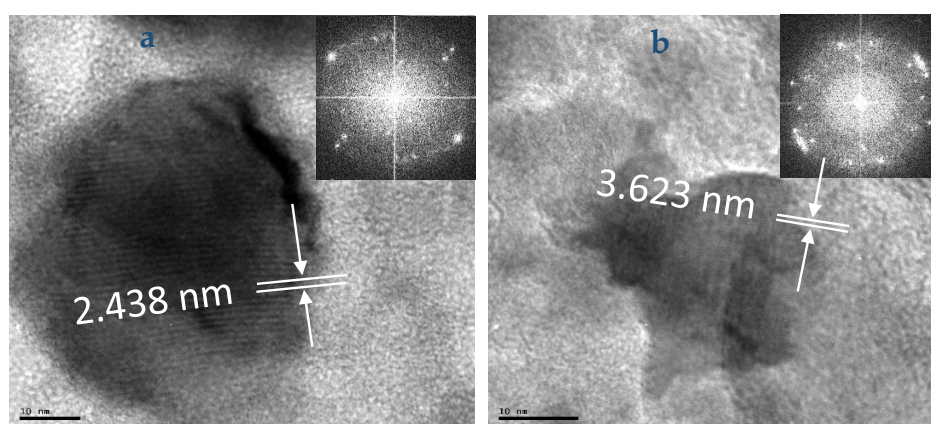
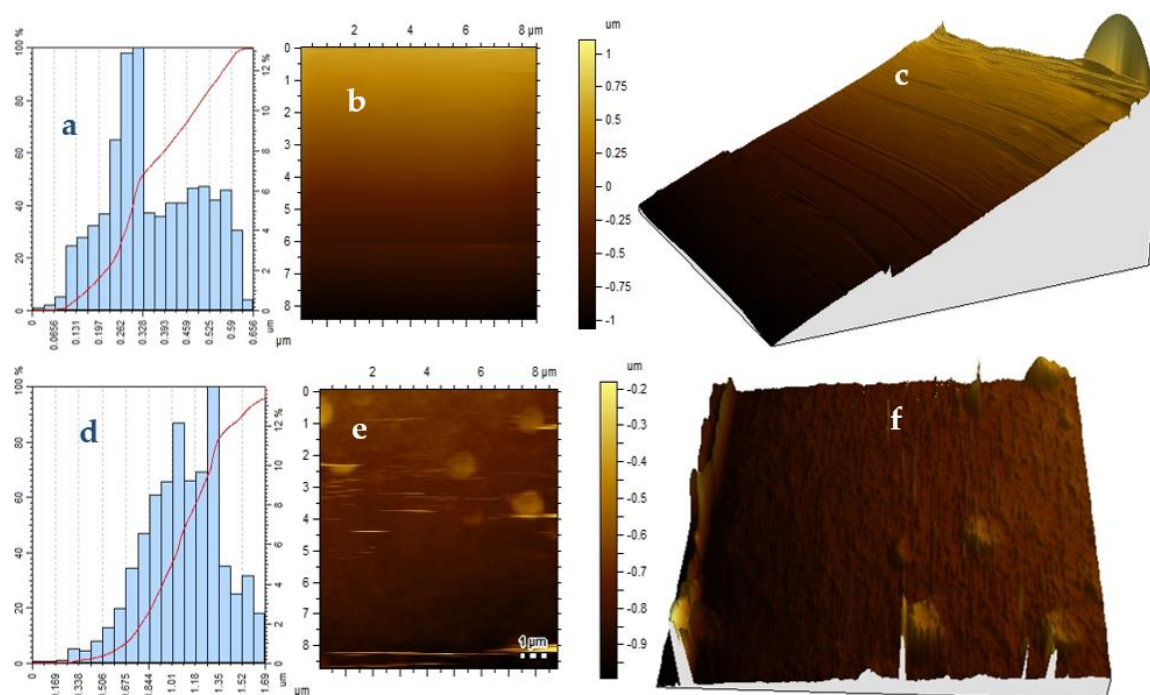


Figure 3. High-resolution transmission electron microscope (HRTEM) images of (a) OCT-PbS and (b) OCT-PbS/HDA nanoparticles.

### 2.3. Atomic Force Microscopy

The surface roughness of the OCT-PbS and OCT-PbS/HDA photosensitizers is indicated by the AFM images (see Figure 4). The AFM results for OCT-PbS/HDA indicate that the molecular precursor route with the HDA capping improves the surface roughness: with TiO<sub>2</sub> photoanode, it is compact and smooth. These results can be linked to the densification and reorganization of the crystallites of the OCT-PbS/HDA film. The photosensitizers exhibited particle size of 0.654  $\mu\text{m}$  for OCT-PbS/HDA and 1.69  $\mu\text{m}$  for OCT-PbS, depicting a regular crystal growth rate. The height clusters of both samples depicted an insignificant change around 0.328 and 1.35  $\mu\text{m}$ , which connotes smaller nanocrystals [35]. The images displayed small spherical nanocrystals with uniform distribution and size in the crystalline phase in both samples, indicating compact nanoparticles [32] and in further agreement with the XRD results.



**Figure 4.** (a–c) Height profile and two-dimensional (2D) and three-dimensional (3D) atomic force microscopy (AFM) images of OCT-PbS/HAD nanoparticles. (d–f) Height profile and 2D and 3D AFM images of OCT-PbS nanoparticles.

### 2.4. Cyclic Voltammetry

In order to evaluate electrocatalytic abilities and the reaction kinetics of PbS/HDA and PbS photosensitizers, the cyclic voltammetry (CV) measurements were adopted with three-electrode systems [36]. The observed CV curves are displayed in Figure 5. In an ideal QDSC, photoexcited electrons from the photosensitizer are injected into the conduction band, and the oxidized photosensitizer is reduced by ions in the electrolyte [37]. The electrocatalytic activity displayed by OCT-PbS/HDA was very low in HI-30 electrolyte due to its overpotential, irreversibility [38] and physisorption. The OCT-PbS sensitizer exhibited significant electrocatalytic activity with stronger current peaks due to a considerable amount of reversibility [39].

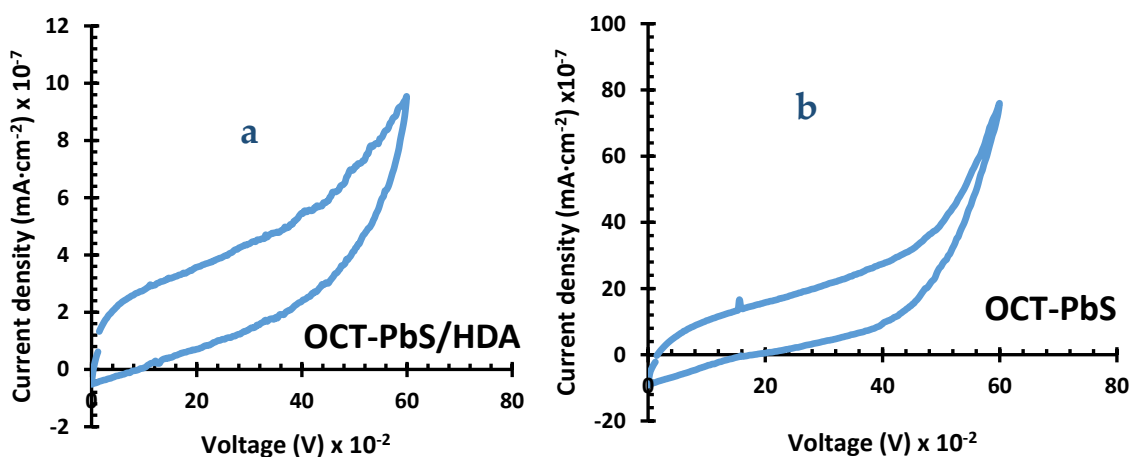


Figure 5. Cyclic voltammetry (CV) spectra of (a) OCT-PbS/HDA and (b) OCT-PbS nanoparticles.

### 2.5. Electrochemical Impedance Spectroscopy Results

Figure 6 shows the EIS measurement. The hemisphere of high-frequency at 100 kHz is for the resistance of charge transport at the counter electrode/electrolyte interface ( $R_1$ ). At low frequencies, the impedance related to the charge transport at the  $\text{TiO}_2/\text{PbS}/\text{electrolyte}$  interface is  $R_2$ . This study focused only on the  $R_2$  to compare the effect of the HDA capping agent on the charge transfer and transport at the  $\text{TiO}_2/\text{PbS}/\text{electrolyte}$  interfaces. The impedance at low frequencies can be pinpointed using  $R_2$ . When the  $R_2$  is lower, the charge transfer is faster at the photosensitizer/electrolyte interface. OCT-PbS/HDA indicated a very poor catalytic activity, which can be linked to the injection of HDA. On the other hand, the OCT-PbS sensitizer displayed lower charge transfer at the photosensitizer/electrolyte interface. This can be linked to the particle size of OCT-PbS sensitizer, which promotes the charge transport speed of the solar cell. This further affirmed the CV and AFM result [40,41]. However,  $R_2$  is also considered as a resistance of charge recombination at the interfaces of  $\text{TiO}_2/\text{QDs}/\text{electrolytes}$ . Decreases in  $R_2$  can boost the charge recombination and shorten electron lifetime, which causes the performance of the solar cell to deteriorate.

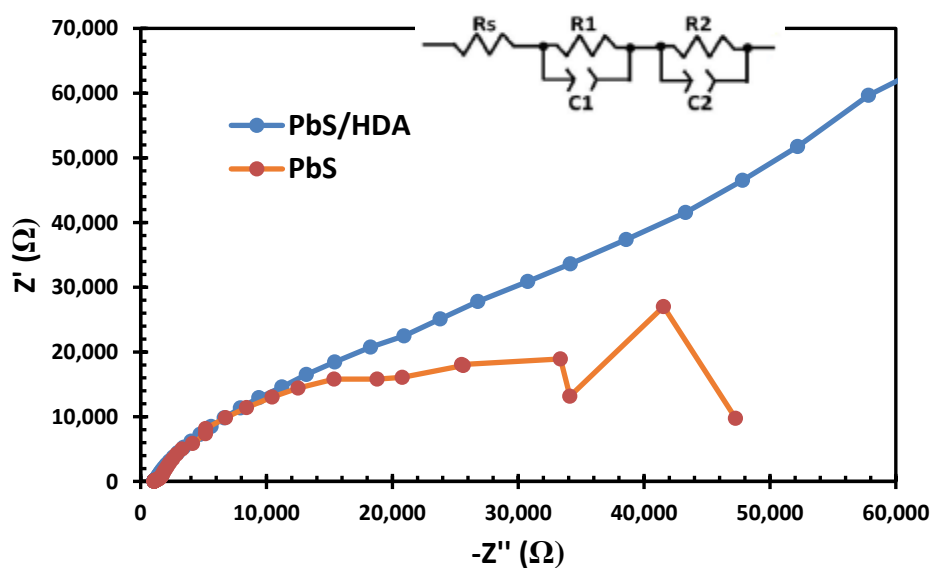


Figure 6. Electrochemical impedance spectroscopy (EIS) spectra of OCT-PbS/HDA and OCT-PbS nanoparticles.



## 2.6. Bode Plot Results of Metal Sulfides Nanoparticles

According to the EIS diagrams, shown in Figure 7, the electron lifetime before the recombination ( $T_r$ ) can be estimated with Equation (1) using the Bode plot.

$$[T_r = 1/(2\pi f_{\max})] \quad (1)$$

The OCT-PbS exhibited a  $T_r$  value of 57 ms. This indicates an increase in electron lifetime and a backreaction reduction of the electron with the injected HI-30 electrolyte. The suppressing of charge recombination implies the longer lifetime of the charge carrier. This leads to better electron collection at the FTO substrate. Based on this study, we can conclude that OCT-PbS displays superior ability compared to OCT-PbS/HDA. Further, the complete coverage of photosensitizers on a photoanode surface is directly linked to their ability to inhibit the charge recombination back to the electrolyte redox couple [42].

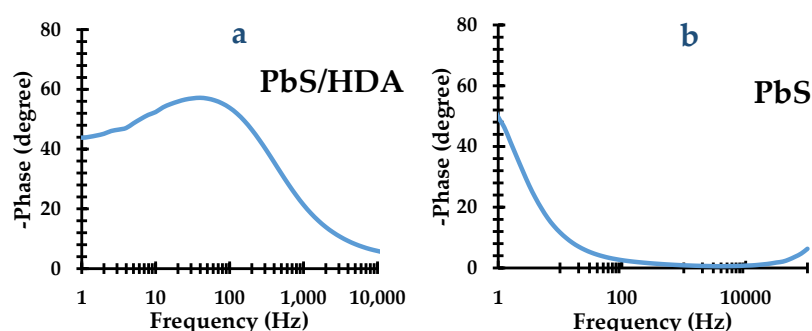


Figure 7. Bode plot spectra of (a) OCT-PbS/HDA and (b) OCT-PbS nanoparticles.

## 2.7. UV-Vis

Figure 8 reveals the absorption spectra of OCT-PbS and OCT-PbS/HDA recorded in the wavelength region from 315 to 535 nm. This implies a low absorbance in the UV region for OCT-PbS and high absorbance in the visible region for OCT-PbS/HDA. The maximum absorption of OCT-PbS is found at 366 nm, and the absorption is found to be 455 nm for OCT-PbS/HDA. The absorption corresponds to an electron excited by a photon of energy, whereby the electron can jump from a lower energy to a higher energy state. The high absorption displayed by Oct-PbS/HDA in the visible region indicates the blue shift. This may be due to quantum confinement. This enables QDSCs to trap the photon energy in the entire UV-Vis spectral region. Wavelengths similar to those obtained in this study for OCT-PbS/HDA have been reported as produced by the recombination of excitons shallowly trapped in electron-hole pairs by [32,43].

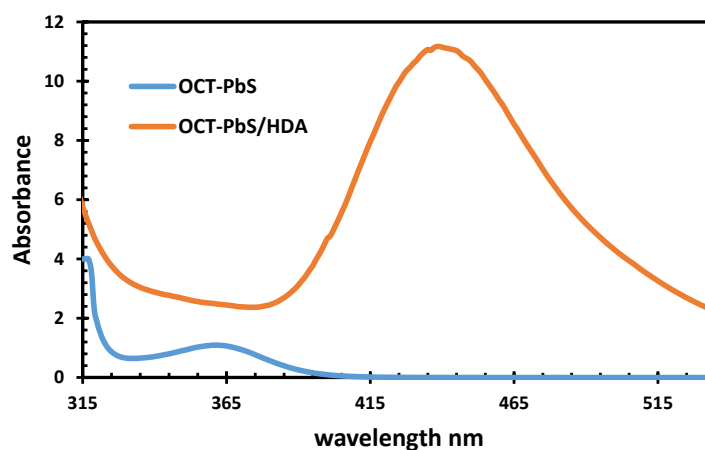


Figure 8. UV-Vis image of OCT-PBS and OCT-PbS/HDA nanoparticles.

## 2.8. J–V Results

Table 1 and Figure 9 illustrate the current-voltage ( $J$ – $V$ ) characteristics of the QDSSCs of OCT-PbS/HDA and OCT-PbS photosensitizers under illumination. A reasonably high short-circuit current density ( $J_{SC}$ ) of 11 mA/cm<sup>2</sup> was observed in the OCT-PbS/HDA QDSSCs, compared to that of the OCT-PbS cells. The nanoporous nature of OCT-PbS/HDA may be related to the high value of  $J_{SC}$ , due to its fabrication by the single-source precursor technique. The values of the open-circuit voltage ( $V_{OC}$ ) (~0.52 V) and efficiency (1.89) for OCT-PbS/HDA proved that the addition of HDA resulted in improved solar cell parameters. The TiO<sub>2</sub> nanoparticle photoanode, with broad size variation and far-field and near-field effect, led to enhancement of  $J_{SC}$  in OCT-PbS/HDA photosensitizer. This also exhibited high absorption of light in the whole visible spectrum. Secondly, recombination was reduced when PbS nanoparticles functioned as electron scavengers [44,45]. The higher electron density in the TiO<sub>2</sub> conduction band could be linked as a factor for higher  $V_{oc}$  value of OCT-PbS/HDA (0.52 V) compared to that of OCT-PbS (0.48 V), which elevated the Fermi level [37]. The FF of QDSSC is usually attributable to the charge transfer resistance at the counter electrode, electron transport resistance through the photoanode, total series resistance of the cell and ion transport resistance [46]. The higher FF of the OCT-PbS (0.74) compared to OCT-PbS/HDA (0.33) was due to the considerable improvement in charge transfer at the counter electrode/electrolyte interface, which reduced the concentration gradients in the electrolyte, internal resistances and the recombination rate, as confirmed by the EIS results [47].

**Table 1.** Current-voltage ( $J$ – $V$ ) curve characteristics of OCT-PbS/HDA and OCT-PbS nanoparticles.

Dye	Photoanode	Electrolyte	CEs	$J_{SC}$ (mA/cm <sup>2</sup> )	$V_{OC}$ (V)	FF	$\eta$ (%)
OCT-PbS/HDA	TiO <sub>2</sub>	HI-30	Pt	11	0.52	0.33	1.89
OCT-PbS	TiO <sub>2</sub>	HI-30	Pt	2.4	0.48	0.74	0.85

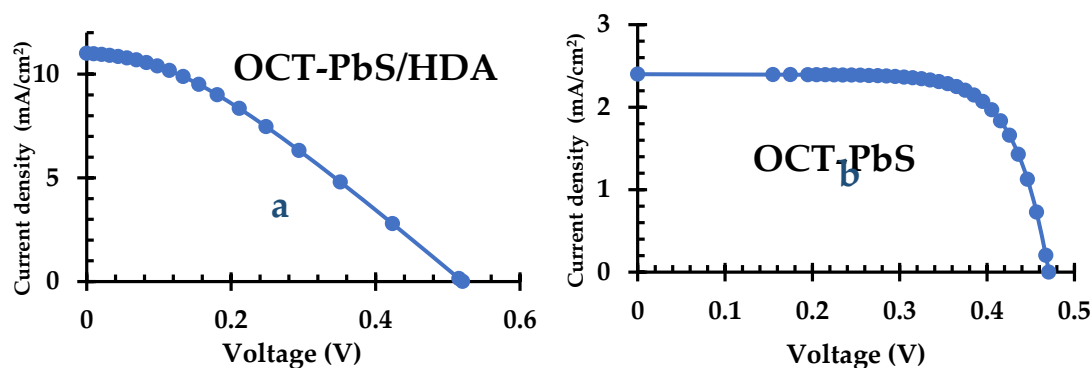


**Figure 9.**  $J$ – $V$  curve characteristics of (a) OCT-PbS/HDA and (b) OCT-PbS nanoparticles.

## 3. Materials and Methods

### 3.1. Material

All materials were purchased from commercial sources and used without further purification. The complete test kits containing fluorine-doped tin oxide (FTO) as glass substrate of TiO<sub>2</sub>, platinum FTO, HI-30 electrolyte iodide, masks, gaskets, chenodeoxycholic acid (CDC) and a hot seal were purchased from Solaronix Company (Aubonne, Switzerland). Additionally, water, oleic acid (OA), methanol, hexadecylamine (HDA), *bis*(*N*-diisopropyl-*N*-octyldithiocarbamate) (OCT) Pb(II) complexes were obtained from Merck (Johannesburg, South Africa).

### 3.2. Synthesis of OCT-PbS/HDA and OCT-PbS Nanoparticles

Nanoparticles were fabricated according to methods in the literature [48]: 0.20 g of *bis*(*N*-diisopropyl-*N*-octyldithiocarbamate) Pb(II) complex was dissolved in 4 mL oleic acid (OA) and injected

into 3 g of hot hexadecylamine (HDA) at 360 °C. An initial temperature of 20–30 °C was attained for the mixture. The reaction was stabilized at 360 °C, and the process lasted for 1 h. The process was allowed to drop to 70 °C, signifying the completion of the process, and about 50 mL of methanol was used to remove excess OA and HDA. Centrifugation was used to separate the flocculent precipitate, which was redispersed with toluene. Low air pressure was used to remove solvent, giving rise to metal sulfides of OCT-PbS/HDA nanoparticles. Synthesis of OCT-PbS nanocrystals was obtained according to the study by a co-worker [49], using (PerkinElmer TGA 4000 thermogravimetric Analyser, San Jose, CA, USA). A portion of 25 mg of the complex was loaded into an alumina pan and weight changes were recorded as a function of temperature for a 10 °C min<sup>-1</sup> temperature gradient between 30–900 °C. A purge gas of flowing nitrogen at a rate of 20 mL min<sup>-1</sup> was used. At temperatures between 360 and 900 °C, the complex end-product was converted into the residue of OCT-PbS nanoparticles from the TGA.

### 3.3. Fabrication and Assembling of Solar Cells

Quantum dot solar cells (QDSC) were prepared with 2 × 2 cm<sup>2</sup> FTO-glass plates of platinum and TiO<sub>2</sub> electrodes, purchased from (Solaronix), with 6 × 6 mm<sup>2</sup> active areas of TiO<sub>2</sub> screen-coated. Dye loading for sensitization was done using 10 mL of warm water with OCT-PbS/HDA and OCT-PbS. Co-adsorbents (co-adsorbent/dye), using chenodeoxycholic acid (CDC), were added. The mediating solution was a commercial HI-30 electrolyte solution (Solaronix, Aubonne, Switzerland), with content of iodide species at 0.05 M. The TiO<sub>2</sub> thin film was soaked in a solution of photosensitizers for 24 h. The two substrates, one coated with TiO<sub>2</sub> loaded with photosensitizers and the other with platinum, were held together using polyethylene and a soldering iron. A syringe was used to inject the HI-30 electrolyte (iodide).

### 3.4. Physical Measurements

An X-ray diffractometer (Cambridge, United Kingdom) was employed to evaluate the structural pattern of the samples; the diffraction structure results were recorded between 10 to 90° at intervals of 0.05°. A JEOL JEM 2100 high-resolution transmission electron microscope (JEOL Inc., Pleasanton, CA, USA) (HRTEM) operating at 200 KV with selected area electron diffraction (SAED) patterns was used. The surface roughness of the OCT-PbS/HDA and OCT-PbS FTO substrates were identified through the use of atomic force microscopy (JPK NanoWizard II AFM, JPK Instruments, Berlin, Germany) in contact mode and a scan rate of 0.8 Hz. Electrochemical studies were evaluated by Metrohm 85,695 Autolab with Nova 1.10 software (Metrohm Johannesburg, South Africa (Pty) Ltd.). A platinum electrode was adopted as a counter electrode. TiO<sub>2</sub> was used as the anode, while HI-30 iodide electrode was utilized as a reference electrode. Cyclic voltammetry (CV) was performed at scan rates between 0.05 to 0.35 V s<sup>-1</sup> with an increment of 0.05 V s<sup>-1</sup>. Electrochemical impedance spectroscopy (EIS) was carried out in the frequency range of 100 kHz to 100 mHz. Current–voltage (*J–V*) parameters were collected through a Keithley 2401 source meter and a Thorax light power meter (RS Components (SA), Johannesburg, South Africa). A Lumixo AM1.5 light simulator was employed, and the lamp was fixed at 50 cm high to avoid illumination outside of the working area. To avoid cell degradation, temperature was kept below 60 °C, and the light power density was kept at 100 mW/cm<sup>-2</sup> (AM1.5). A PerkinElmer Lambda 25 UV–Vis spectrophotometer was employed to carry out observations of optical absorption properties at room temperature (PerkinElmer, Inc. Waltham, MA, USA).

## 4. Summary and Conclusions

In summary, the fabrication of inorganic PbS sensitizers through the molecular precursor route and their application in photovoltaic cells were investigated in this study. PbS photosensitizers deposited on TiO<sub>2</sub> by direct deposition revealed the structure, morphologies and electrocatalytic activity of a typical PbS nanocrystalline structure and displayed uniform size-distribution. The SAED of OCT-PbS and OCT-PbS/HDA confirmed the polycrystalline nature of both materials. The AFM results of OCT-PbS/HDA suggested that the injection of the HDA capping agent improved the surface



roughness of the materials with TiO<sub>2</sub> photoanode. Electrocatalytic activity of OCT-PbS was enhanced in HI-30 electrolyte compared to the OCT-PbS/HDA sensitizer and exhibited significant electrocatalytic activity. The OCT-PbS/HDA sensitizer exhibited a strong resistance interaction with the electrolyte, indicating poor catalytic activity, compared to the OCT-PbS sensitizer. The better conversion efficiency displayed by OCT-PbS/HDA proved its superiority as a good sensitizer, and this is strongly linked to its nanoporous nature and electrocatalytic activity. The addition of an HDA capping agent has made a great improvement to the conversion efficiency of OCT-PbS/HDA.

**Author Contributions:** Conceptualization, J.Z.M., M.A.A., and E.L.M.; methodology, J.Z.M., M.A.A., and E.L.M.; validation, J.Z.M., M.A.A., and E.L.M.; formal analysis, J.Z.M., M.A.A., and E.L.M.; investigation, M.A.A., resources, J.Z.M., M.A.A., and E.L.M.; data curation, J.Z.M., M.A.A., and E.L.M.; writing—original draft preparation M.A.A., writing—review and editing M.A.A., visualization, M.A.A.; supervision, J.Z.M., and E.L.M.; funding acquisition, J.Z.M.; and E.L.M. All authors have read and agreed to the published version of the manuscript.

**Funding:** This research was funded by the National Department of Science and Innovation (DST/CON 0170/2019), National Research Foundation (GUN: 93215), Govan Mbeki Research and Development Centre (GMRDC) at the University of Fort Hare, South Africa, Eskom TESP (P948) and Thuthuka Grant (GUN: 118139).

**Acknowledgments:** The authors appreciate the support from Kwabena Manu (Kbizz IT support) for the visualization of data and thank the Energy, Materials and Inorganic Chemistry Research Group (EMICREG) at the university of Fort Hare for allowing to use of their laboratory, materials and instruments.

**Conflicts of Interest:** The authors declare no conflict of interest.

## References

1. Rath, T.; Trimmel, G. In situ syntheses of semiconducting nanoparticles in conjugated polymer matrices and their application in photovoltaics. *Hybrid Mater.* **2015**, *1*. [[CrossRef](#)]
2. Meyer, E.L.; Mbese, J.Z.; Agoro, M.A. The Frontiers of Nanomaterials (SnS, PbS and CuS) for Dye-Sensitized Solar Cell Applications: An Exciting New Infrared Material. *Molecules* **2019**, *24*, 4223. [[CrossRef](#)]
3. Reynolds, L.X.; Lutz, T.; Dowland, S.; MacLachlan, A.; King, S.; Haque, S.A. Charge photogeneration in hybrid solar cells: A comparison between quantum dots and in situ grown CdS. *Nanoscale* **2012**, *4*, 1561–1564. [[CrossRef](#)] [[PubMed](#)]
4. Zhou, Y.; Eck, M.; Men, C.; Rauscher, F.; Niyamakom, P.; Yilmaz, S.; Dumsch, I.; Allard, S.; Scherf, U.; Krüger, M. Efficient polymer nanocrystal hybrid solar cells by improved nanocrystal composition. *Sol. Energy Mater. Sol. Cells* **2011**, *95*, 3227–3232. [[CrossRef](#)]
5. Luo, K.; Wu, W.; Xie, S.; Jiang, Y.; Liao, S.; Qin, D. Building Solar Cells from Nanocrystal Inks. *Appl. Sci.* **2019**, *9*, 1885. [[CrossRef](#)]
6. Chen, H.C.; Lai, C.W.; Wu, I.C.; Pan, H.R.; Chen, I.W.; Peng, Y.K.; Liu, C.L.; Chen, C.H.; Chou, P.T. Enhanced performance and air stability of 3.2% hybrid solar cells: How the functional polymer and CdTe nanostructure boost the solar cell efficiency. *Adv. Mater.* **2011**, *23*, 5451–5455. [[CrossRef](#)]
7. Rong, Z.; Guo, X.; Lian, S.; Liu, S.; Qin, D.; Mo, Y.; Xu, W.; Wu, H.; Zhao, H.; Hou, L. Interface Engineering for Both Cathode and Anode Enables Low-Cost Highly Efficient Solution-Processed CdTe Nanocrystal Solar Cells. *Adv. Funct. Mater.* **2019**, *29*, 1904018. [[CrossRef](#)]
8. Dogan, S.; Bielewicz, T.; Lebedeva, V.; Klinke, C. Photovoltaic effect in individual asymmetrically contacted lead sulfide nanosheets. *Nanoscale* **2015**, *7*, 4875–4883. [[CrossRef](#)]
9. Zhao, N.; Osedach, T.P.; Chan, L.Y.; Geyer, S.M.; Wanger, D.; Binda, M.T.; Arango, A.C.; Bawendi, M.G.; Bulovic, V. Colloidal PbS quantum dot solar cells with high fill factor. *ACS Nano* **2010**, *4*, 3743–3752. [[CrossRef](#)]
10. Onwudiwe, D.C. Microwave-assisted synthesis of PbS nanostructures. *Heliyon* **2019**, *5*, e01413. [[CrossRef](#)]
11. Davar, F.; Mohammadikish, M.; Loghman-Estarki, M.R.; Masteri-Farahani, M. Synthesis of micro- and nanosized PbS with different morphologies by the hydrothermal process. *Ceram. Int.* **2014**, *40*, 8143–8148. [[CrossRef](#)]
12. Mamiyev, Z.Q.; Balayeva, N.O. Preparation and optical studies of PbS nanoparticles. *Opt. Mater.* **2015**, *46*, 522–525. [[CrossRef](#)]
13. Goswami, S.K.; Oh, E. Morphology control and photovoltaic application of solvothermally synthesized PbS nanostructures. *Mater. Lett.* **2014**, *117*, 138–141.

14. Zhao, Z.; Zhang, J.; Dong, F.; Yang, B. Supercrystal structures of polyhedral PbS nanocrystals. *J. Colloid Interface Sci.* **2011**, *359*, 351–358. [[CrossRef](#)]
15. Zhao, Z.; Zhang, K.; Zhang, J.; Yang, K.; He, C.; Dong, F.; Yang, B. Synthesis of size and shape-controlled PbS nanocrystals and their self-assembly. *Colloids Surf. A Physicochem. Eng. Asp.* **2010**, *355*, 114–120. [[CrossRef](#)]
16. Kumar, D.; Agarwal, G.; Tripathi, B.; Vyas, D.; Kulshrestha, V. Characterization of PbS nanoparticles synthesized by chemical bath deposition. *J. Alloys Compd.* **2009**, *484*, 463–466. [[CrossRef](#)]
17. Kowshik, M.; Vogel, W.; Urban, J.; Kulkarni, S.K.; Paknikar, K.M. Microbial synthesis of semiconductor PbS nanocrystallites. *Adv. Mater.* **2002**, *14*, 815–818. [[CrossRef](#)]
18. Zhengping, Q.; Yi, X.; Yingjie, Z.; Yitai, Q. Synthesis of PbS/poly (vinyl acetate) nanocomposites by  $\gamma$ -irradiation. *Mater. Sci. Eng. B* **2000**, *77*, 144–146. [[CrossRef](#)]
19. Nyamen, L.D.; Pullabhotla, V.S.; Nejo, A.A.; Ndifon, P.; Revaprasadu, N. Heterocyclic dithiocarbamates: Precursors for shape-controlled growth of CdS nanoparticles. *New J. Chem.* **2011**, *35*, 1133–1139. [[CrossRef](#)]
20. Nyamen, L.D.; Revaprasadu, N.; Pullabhotla, R.V.; Nejo, A.A.; Ndifon, P.T.; Malik, M.A.; O'Brien, P. Synthesis of multi-podal CdS nanostructures using heterocyclic dithiocarbamate complexes as precursors. *Polyhedron* **2013**, *56*, 62–70. [[CrossRef](#)]
21. Kun, W.N.; Mlowe, S.; Nyamen, L.D.; Ndifon, P.T.; Malik, M.A.; Munro, O.Q.; Revaprasadu, N. Heterocyclic Bismuth(III) Dithiocarbamate Complexes as Single-Source Precursors for the Synthesis of Anisotropic Bi<sub>2</sub>S<sub>3</sub> Nanoparticles. *Chem. Eur. J.* **2016**, *22*, 13127–13135. [[CrossRef](#)] [[PubMed](#)]
22. Roffey, A.; Hollingsworth, N.; Islam, H.U.; Mercy, M.; Sankar, G.; Catlow, C.R.; Hogarth, G.; de Leeuw, N.H. Phase control during the synthesis of nickel sulfide nanoparticles from dithiocarbamate precursors. *Nanoscale* **2016**, *8*, 11067–11075. [[CrossRef](#)] [[PubMed](#)]
23. Uflyand, I.E.; Dzhardimalieva, G.I. Nanomaterials Preparation by Thermolysis of Metal Chelates. In *Thermolysis of Metal Chelates in Polymer Matrices*; Springer: Berlin, Germany, 2018; pp. 425–458. ISBN 978-3-319-93404-4.
24. Fikai, D.; Grumezescu, A.M. Dendrimers and dendronized materials as nanocarriers. In *Nanostructures for Novel Therapy: Synthesis, Characterization and Applications*; Elsevier: Amsterdam, The Netherlands, 2017; p. 429. ISBN 9780323461481.
25. Dzhardimalieva, G.I.; Uflyand, I.E. Chalcogen-containing metal chelates as single-source precursors of nanostructured materials: Recent advances and future development. *J. Coord. Chem.* **2019**, *72*, 1425–1465. [[CrossRef](#)]
26. Agoro, M.A.; Meyer, E.L.; Mbese, J.Z.; Manu, K. Electrochemical Fingerprint of CuS-Hexagonal Chemistry from (Bis(N-1,4-Phenyl-N-(4-Morpholinedithiocarbamate) Copper(II) Complexes) as Photon Absorber in Quantum-Dot/Dye-Sensitised Solar Cells. *Catalysts* **2020**, *10*, 300. [[CrossRef](#)]
27. Mbese, J.Z.; Meyer, E.L.; Agoro, M.A. Electrochemical Performance of Photovoltaic Cells using HDA Capped-SnS Nanocrystal from bis (N-1,4-Phenyl-N-Morpho-Dithiocarbamate) Sn(II) Complexes. *Nanomaterials* **2020**, *10*, 414. [[CrossRef](#)]
28. Moreno, O.P.; Pérez, R.G.; Merino, R.P.; Portillo, M.C.; Téllez, G.H.; Rosas, E.R. Optical and structural properties of PbSn<sup>3+</sup> nanocrystals grown by chemical bath. *Thin Solid Films* **2016**, *616*, 800–807. [[CrossRef](#)]
29. Portillo, M.C.; Moreno, O.P.; Pérez, R.G.; Merino, R.P.; Juarez, H.S.; Cuapa, S.T.; Rosas, E.R. Characterization and growth of doped-PbS in situ with Bi<sup>3+</sup>, Cd<sup>2+</sup> and Er<sup>3+</sup> ions by chemical bath. *Mater. Sci. Semicond. Process.* **2017**, *72*, 22–31. [[CrossRef](#)]
30. Dasgupta, N.P.; Lee, W.; Prinz, F.B. Atomic layer deposition of lead sulfide thin films for quantum confinement. *Chem. Mater.* **2009**, *21*, 3973–3978. [[CrossRef](#)]
31. Portillo-Moreno, O.; Gutiérrez-Pérez, R.; Chávez Portillo, M.; Specia, M.; Hernández-Téllez, G.; Lazcano Hernández, M.; Moreno Rodríguez, A.; Palomino-Merino, R.; Rubio Rosas, E. Growth of doped PbS: Co<sup>2+</sup> nanocrystals by Chemical Bath. *Rev. Mex. Fis.* **2016**, *62*, 456–460.
32. Palomino Merino, R.; Gutiérrez Pérez, R.; Trejo García, P.; Chaltel Lima, L.; Portillo Moreno, O.; Araiza García, M.E.; Moreno Rodríguez, A.; Rubio Rosas, E. Influence of L-Tryptophan on Growth and Optical Properties of PbS Nanocrystalline Thin Films. *J. Nanomater.* **2018**, 3431942. [[CrossRef](#)]
33. Dong, Y.; Wen, J.; Pang, F.; Luo, Y.; Peng, G.D.; Chen, Z.; Wang, T. Formation and photoluminescence property of PbS quantum dots in silica optical fiber based on atomic layer deposition. *Opt. Mater. Express.* **2015**, *5*, 712–719. [[CrossRef](#)]

34. Khan, A.H.; Maji, S.; Chakraborty, S.; Manik, N.B.; Acharya, S. Multidimensional self-assembly of peanut shaped PbS nanostructures. *RSC Adv.* **2012**, *2*, 186–191. [[CrossRef](#)]
35. Saraidarov, T.; Gevorgian, A.; Reisfeld, R.; Sashchiuk, A.; Bashouti, M.; Lifshitz, E. Synthesis, structural and electrical characterization of PbS NCs in titania sol–gel films. *J. Sol-Gel Sci. Technol.* **2007**, *44*, 87–95. [[CrossRef](#)]
36. Li, L.; Yang, X.; Zhao, J.; Gao, J.; Hagfeldt, A.; Sun, L. Efficient organic dye sensitized solar cells based on modified sulfide/polysulfide electrolyte. *J. Mater. Chem.* **2011**, *21*, 5573–5575. [[CrossRef](#)]
37. Lee, Y.L.; Chang, C.H. Efficient polysulfide electrolyte for CdS quantum dot-sensitized solar cells. *J. Power Sources* **2008**, *185*, 584–588. [[CrossRef](#)]
38. Radich, J.G.; Dwyer, R.; Kamat, P.V. Cu<sub>2</sub>S reduced graphene oxide composite for high-efficiency quantum dot solar cells. Overcoming the redox limitations of S<sup>2-</sup>/Sn<sup>2-</sup> at the counter electrode. *J. Phys. Chem. Lett.* **2011**, *2*, 2453–2460. [[CrossRef](#)]
39. Gopi, C.V.; Bae, J.H.; Venkata-Haritha, M.; Kim, S.K.; Lee, Y.S.; Sarat, G.; Kim, H.J. One-step synthesis of solution processed time-dependent highly efficient and stable PbS counter electrodes for quantum dot-sensitized solar cells. *RSC Adv.* **2015**, *5*, 107522–107532. [[CrossRef](#)]
40. Han, L.; Koide, N.; Chiba, Y.; Islam, A.; Komiyama, R.; Fuke, N.; Fukui, A.; Yamanaka, R. Improvement of efficiency of dye-sensitized solar cells by reduction of internal resistance. *Appl. Phys. Lett.* **2005**, *86*, 213501. [[CrossRef](#)]
41. Chen, Y.; Zhang, X.; Tao, Q.; Fu, W.; Yang, H.; Su, S.; Mu, Y.; Zhou, L.; Li, M. High catalytic activity of a PbS counter electrode prepared via chemical bath deposition for quantum dots-sensitized solar cells. *RSC Adv.* **2015**, *5*, 1835–1840. [[CrossRef](#)]
42. Punnoose, D.; Suh, S.M.; Kim, B.J.; Kumar, C.S.P.; Rao, S.S.; Thulasi-Varma, C.V.; Reddy, A.E.; Chung, S.H.; Kim, H.J. The influence of in situ deposition techniques on PbS seeded CdS/CdSe for enhancing the photovoltaic performance of quantum dot sensitized solar cells. *J. Electroanal. Chem.* **2016**, *773*, 27–38. [[CrossRef](#)]
43. Salavati-Niasari, M.; Ghanbari, D.; Loghman-Estarki, M.R. Star-shaped PbS nanocrystals prepared by hydrothermal process in the presence of thioglycolic acid. *Polyhedron* **2012**, *35*, 149–153. [[CrossRef](#)]
44. Bhardwaj, S.; Pal, A.; Chatterjee, K.; Rana, T.H.; Bhattacharya, G.; Roy, S.S.; Chowdhury, P.; Sharma, G.D.; Biswas, S. Significant enhancement of power conversion efficiency of dye-sensitized solar cells by the incorporation of TiO<sub>2</sub>–Au nanocomposite in TiO<sub>2</sub> photoanode. *J. Mater. Sci.* **2018**, *53*, 8460–8473.
45. Bhardwaj, S.; Pal, A.; Chatterjee, K.; Rana, T.H.; Bhattacharya, G.; Roy, S.S.; Chowdhury, P.; Sharma, G.D.; Biswas, S. Enhanced efficiency of PbS quantum dot-sensitized solar cells using plasmonic photoanode. *J. Nanopart. Res.* **2018**, *20*, 198. [[CrossRef](#)]
46. Tachan, Z.; Shalom, M.; Hod, I.; Ruhle, S.; Tirosh, S.; Zaban, A. PbS as a highly catalytic counter electrode for polysulfide-based quantum dot solar cells. *J. Phys. Chem. Lett.* **2011**, *115*, 6162–6166. [[CrossRef](#)]
47. Kim, H.J.; Kim, S.W.; Gopi, C.V.; Kim, S.K.; Rao, S.S.; Jeong, M.S. Improved performance of quantum dot-sensitized solar cells adopting a highly efficient cobalt sulfide/nickel sulfide composite thin film counter electrode. *J. Power Sources* **2014**, *268*, 163–170. [[CrossRef](#)]
48. Mbese, J.Z.; Ajibade, P.A.; Matebese, F.; Agoro, M.A. Optical and Structural Properties of TOPO/HDA Capped Cus Nanocrystals via Thermal Decomposition of Bis(N-Diisopropylthiocarbamate) Cu(II) Complex. *J. Nano Res.* **2019**, *59*, 161–165. [[CrossRef](#)]
49. Meyer, E.L.; Mbese, J.Z.; Agoro, M.A.; Taziwa, T. Optical and structural-chemistry of SnS nanocrystals prepared by thermal decomposition of bis(N-di-isopropyl-N-octylthiocarbamate)tin(II) complex for promising materials in solar cell applications. *Opt. Quant. Electron.* **2020**, *52*, 2–11. [[CrossRef](#)]

**Sample Availability:** Samples of the compounds are not available from the authors.



© 2020 by the authors. Licensee MDPI, Basel, Switzerland. This article is an open access article distributed under the terms and conditions of the Creative Commons Attribution (CC BY) license (<http://creativecommons.org/licenses/by/4.0/>).